Available online at www.sciencedirect.com
SCIENCE DIRECT®
International Journal of Heat and Mass Transfer 48 (2005) 647–664
International Journal of HEAT and MASS TRANSFER
www.elsevier.com/locate/ijhmt

Enhancement of forced-convection cooling of multiple heated blocks in a channel using porous covers

P.C. Huang [a,*], C.F. Yang [a], J.J. Hwang [b], M.T. Chiu [b]

[a] *Department of Air-Conditioning and Refrigerating Engineering, National Taipei University of Technology, Taipei, Taiwan 106, Republic of China*

[b] *Department of Mechanical Engineering, National Sun Yat-Sen University, Kaohsiung, Taiwan 804, Republic of China*

Received 22 January 2003; received in revised form 2 July 2004
Available online 21 November 2004

Abstract

A numerical study was carried out for enhanced heat transfer from multiple heated blocks in a channel by porous covers. The flow field is governed by the Navier–Stokes equation in the fluid region, the Darcy–Brinkman–Forchheimer equation in the porous region, and the thermal field by the energy equation. Solution of the coupled governing equations is obtained using a stream function-vorticity analysis. This study details the effects of variations in the Darcy number, Reynolds number, inertial parameter, and two pertinent geometric parameters, to illustrate important fundamental and practical results. The results show that the recirculation caused by porous-covering block will significantly enhance the heat transfer rate on both top and right faces of second and subsequent blocks.

Keywords: Porous cover; Darcy number; Recirculation

1. Introduction

Considerable attention has been given to thermal control of electronic equipment and devices in the past decades due to the requirement of the maintenance of relatively constant electronic component temperature equal to or below a maximum operation temperature. Studies have shown that a significant change in the design temperature can lead to a perceptible reduction in the reliability of the electronic components [1]. Different high-effective cooling techniques [2] have been used in the past to obtain heat transfer enhancement with a minimum of frictional losses including the traditional methods of natural and forced convective cooling. One of the promising techniques is the application of a porous material. This is due to the high ratio of surface area to volume in the heat transfer process and the enhanced flow mixing, caused by the tortuous path of the porous matrix, in the thermal dispersion process.

Transport phenomena through porous media has been of continuing interest due to its relevance in diverse engineering applications. Such applications include the thermal insulation, geothermal energy systems, heat exchanger, enhanced oil recovery, drying processes, and unclear waste disposal. Porous media is also utilized in applications such as heat pipe technology, industrial furnace, cooling of electronic equipment, and fixed-bed nuclear propulsion.

The problem of forced convection enhancement in a channel fully or partially packed with a porous or

* Corresponding author. Tel.: +886 2 2771 2171x3514; fax: +886 2 2731 4919.
E-mail address: pchuang@ntut.edu.tw (P.C. Huang).

0017-9310/$ - see front matter © 2004 Elsevier Ltd. All rights reserved.
doi:10.1016/j.ijheatmasstransfer.2004.07.041

Nomenclature

A	dimensionless geometric parameter of porous cover, W_p^*/H_p^*
B	dimensionless geometric parameter of porous cover, S_p^*/W_p^*
Da	Darcy number, K/R^2
F	a function that depends on the Reynolds number and the microstructure of the porous medium, used in expressing inertia terms
h	convective heat transfer coefficient (W/m^2 K)
H_p	height of porous cover (m)
H_s	height of the solid block (m)
k	thermal conductivity (W/m K)
K	permeability of the porous medium (m^2)
L_e	length of channel upstream from the porous-block array (m)
L_o	length of channel downstream from the porous-block array (m)
L	length of the channel as shown in Fig. 1a, (m)
Nu	Nusselt number, hx/k_f
Pr	Prandtl number, v/α
Q	heat generation per unit length in each block (W/m)
R	height of channel (m)
Re	Reynold number, $u_{av}R/v$
R_k	thermal conductivity ratio, k_s/k_f or k_{eff}/k_f
S_p	spacing between porous-covering blocks (m)
S_s	spacing between solid blocks (m)
T	temperature (K)
u	x-component velocity (m/s)
v	y-component velocity (m/s)
V	velocity vector (m/s)
W_p	width of porous cover (m)
W_s	width of solid block (m)
x	horizontal coordinate (m)
y	vertical coordinate (m)

Greek symbols

α	thermal diffusivity (m^2/s)
α_{eff}	effective thermal diffusivity, $k_{eff}/\rho_f c_{p,f}$ (m^2/s)
ε	porosity of the porous medium
Λ	inertial parameter, $FR\epsilon/\sqrt{K}$
μ	dynamic viscosity (kg/m s)
v	kinematic viscosity (m^2/s)
ξ	vorticity (1/s)
Π	overall exposed area of a block (m^2)
φ	stream function (m^2/s)

Superscript

*	dimensionless quantity

Subscripts

eff	effective
f	fluid
m	overall mean
p	porous
s	solid
x	local
e	condition at inlet

fibrous material has been studied extensively in the literature. Koh and Colony [3] analyzed the cooling effectiveness for a porous material in a cooling passage. Kaviany [4] studied heat transfer in porous media bounded by two isothermal parallel plates in laminar forced convection. Huang and Vafai [5] numerically simulated forced convection problem in an isothermal parallel plate channel with porous block array. Recently, Zhang et al. [6] performed a numerical study on the enhancement of combined convective and radioactive heat transfer using a porous core in a circular duct.

Among these studies, the heat transfer of a fully/partially porous channel with discrete heated sources was of special interest due to its applications on the cooling of electronics. Kuo and Tien [7] solved the problem of forced convection in a porous channel with discrete heat sources on one wall. They reported a two to four times increase of heat transfer as compared to that of slug-flow in a clear duct. Rizk and Kleinstreuer [8] analyzed laminar forced convection on discrete heated blocks in a porous channel and showed an increase in heat transfer when compared with the nonporous channel. Hadim [9] investigated forced convection in a channel fully or partially filled with the porous medium and containing discrete heat sources on the bottom wall. A significant increase in heat transfer rate was observed as the Darcy number was decrease, especially at the leading edge of each heat source. Ould-Amer et al. [10] analyzed the effect of porous insert between the heated blocks. They showed that porous insert enhance the heat transfer rate on the vertical sides of the blocks. Most of these studies relate to the aspect of forced convection over the porous/fluid composite system, however, little is known about the problem combining forced convection in a fluid/porous composite system and conduction in the solid region due to the complex geometry and the different thermal properties among the composite system. This constitutes a case for forced convection over a fluid/porous/solid composite system, such as a finite-sized porous substance enclosing a block where the block is used to simulate heated electronic component while the porous cover simulate the porous heat sink.

This paper presents a numerical investigation of forced convective cooling enhancement of a two-dimensional array of multiple heated blocks located upon lower plate of an insulated channel utilizing the porous covers. In this work the basic interaction phenomena between the porous substrate and the fluid region for these fluid/porous/solid composite system as well as the methodology for enhancing the heat transfer rate around the exposed block faces have been analyzed. Furthermore, the influences of various parameters governing the hydrodynamic and thermal characteristics of the problem are examined to establish the fundamental effects and provide practical results. It is shown that specific choices in certain governing parameters, such as the size, space, or permeability of the porous cover, can have significant effects on the cooling of the blocks.

2. Analysis and formulation

The configuration of problem under investigation is depicted in Fig. 1(a). It includes flow through a parallel-plate channel with multiple porous-covering heated blocks on the bottom plate. Both upper and lower channel walls are insulated. The fluid enters the channel at uniform temperature T_e with a parabolic velocity profile. The flow is assumed to be steady, incompressible, and two-dimensional. Buoyancy induced effects are assumed negligible, and the heat generation within the blocks is assumed to be constant and uniform. Besides, the thermophysical properties of the fluid and the porous matrix are assumed to be constant, and the fluid-saturated porous medium is considered homogeneous, isotropic, nondeformable, and in local thermodynamic equilibrium with the fluid. Possible channelling near the wall is neglected in the present study because fibrous media are considered for which the porosity and permeability are relatively constant even close to the wall [11]. In this work, the flow is modelled by the Darcy–Brinkman–Forchheimer equation in the porous matrix to incorporate the viscous and inertial effects [12] and by Navier–Stokes equation in the fluid domain, and the thermal field by the energy equation. Then, an efficient alternative method for combining the three sets of governing

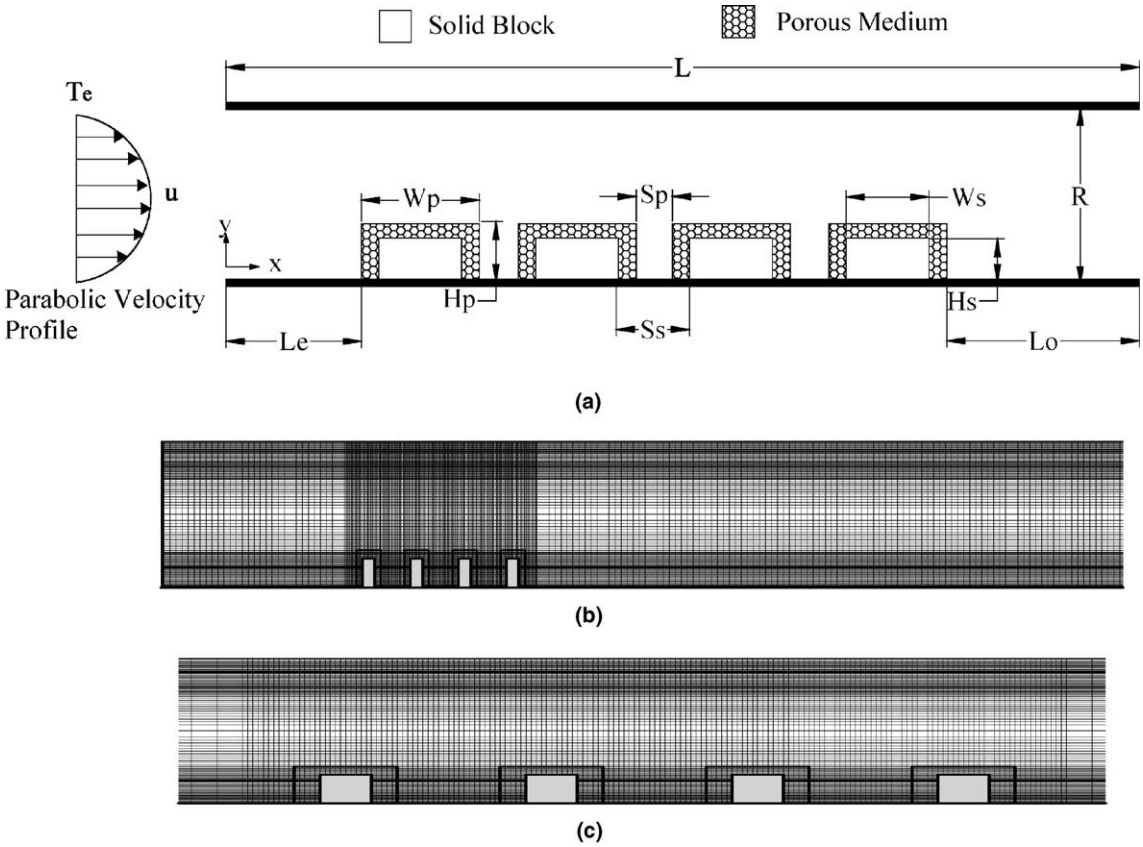

Fig. 1. (a) Schematic diagram of the multiple porous-covering heat block problem, (b) a typical non-uniform grid system for the whole computational domain, and (c) a close-up of the region near the porous-covering block array.

equations for the fluid, porous, and solid regions into one set of conservation equations is to model the whole fluid/porous/solid composite system as a single domain governed by one set of conservations, the solution of which satisfies the matching conditions at both fluid/porous and porous/solid interfaces. The above-mentioned resulting momentum and energy equations in terms of dimensionless variables are as followings [5]:

$$\frac{\partial\varphi^*}{\partial y^*}\frac{\partial\xi^*}{\partial x^*}-\frac{\partial\varphi^*}{\partial x^*}\frac{\partial\xi^*}{\partial y^*}=\frac{1}{Re}\nabla^2\xi^*+S^*_\varphi \tag{1}$$

$$\nabla^2\varphi^*=-\xi^* \tag{2}$$

$$Pe\left(\frac{\partial\varphi^*}{\partial y^*}\frac{\partial T^*}{\partial x^*}-\frac{\partial\varphi^*}{\partial x^*}\frac{\partial T^*}{\partial y^*}\right)=R_k\nabla^2T^*+\frac{\vartheta}{H^*\cdot W^*} \tag{3}$$

where (x^*,y^*) are dimensionless rectangular Cartesian coordinates, R_k is the thermal conductivity ratio, ϑ is a function set equal to one to account for heat generation in the block, and to zero elsewhere, and φ and ξ are the stream function and vorticity, respectively, which are related to the fluid velocity components u and v by

$$u=\frac{\partial\varphi}{\partial y},\quad v=-\frac{\partial\varphi}{\partial x},\quad \xi=\frac{\partial v}{\partial x}-\frac{\partial u}{\partial y} \tag{4}$$

The non-dimensional parameters in the fluid region are

$$\begin{aligned}&Re_{\mathrm{f}}=\frac{u_{\mathrm{av}}R}{v_{\mathrm{f}}},\quad Pe_{\mathrm{f}}=\frac{u_{\mathrm{av}}R}{\alpha_{\mathrm{f}}},\\&R_k=1,\quad \vartheta=0,\quad S^*_\varphi=0\end{aligned} \tag{5}$$

and in the porous region the non-dimensional parameters are

$$\begin{aligned}&Re_{\mathrm{eff}}=\frac{u_{\mathrm{av}}R}{v_{\mathrm{eff}}},\quad Pe_{\mathrm{eff}}=\frac{u_{\mathrm{av}}R}{\alpha_{\mathrm{eff}}},\\&S^*_\varphi=-\frac{1}{Re_{\mathrm{eff}}Da}\xi^*-\Lambda|\vec{V}^*|\xi^*-\Lambda\left[v^*\frac{\partial|\vec{V}^*|}{\partial x^*}-u^*\frac{\partial|\vec{V}^*|}{\partial y^*}\right]\end{aligned} \tag{6}$$

$$Da=\frac{K}{R^2},\quad \Lambda=\frac{FR\varepsilon}{\sqrt{K}},\quad R_k=\frac{k_{\mathrm{eff}}}{k_{\mathrm{f}}},\quad \vartheta=0 \tag{7}$$

and in the solid-block region since the solid is stationary, only the energy equation needs to be considered. Then the energy equation for solid blocks becomes

$$R_k\nabla^2T^*+\frac{\vartheta}{H^*\cdot W^*}=0 \tag{8}$$

where $R_k=\frac{k_{\mathrm{s}}}{k_{\mathrm{f}}}$ (taken equal to 10 in the present study), $\vartheta=1$. The source term s^*_φ can be considered as those contributing to the vorticity generation due to the presence of the rectangular porous-covering blocks. All of the above variables have been non-dimensionalized based on the following definitions:

$$\begin{aligned}&x^*=\frac{x}{R},\quad y^*=\frac{y}{R},\quad u^*=\frac{u}{u_{\mathrm{av}}},\quad v^*=\frac{v}{u_{\mathrm{av}}},\\&|\vec{V}^*|=\sqrt{u^{*2}+v^{*2}},\quad L^*=\frac{L}{R},\\&H^*_{\mathrm{p}}=\frac{H_{\mathrm{p}}}{R},\quad W^*_{\mathrm{p}}=\frac{W_{\mathrm{p}}}{R}\end{aligned} \tag{9}$$

$$\begin{aligned}&H^*_{\mathrm{s}}=\frac{H_{\mathrm{s}}}{R},\quad W^*_{\mathrm{s}}=\frac{W_{\mathrm{s}}}{R},\quad \varphi^*=\frac{\varphi}{u_{\mathrm{av}}R},\quad \xi^*=\frac{R\xi}{u_{\mathrm{av}}},\\&T^*=\frac{T-T_{\mathrm{e}}}{Q/k_{\mathrm{f}}},\quad Pr=\frac{v}{\alpha},\quad P^*=\frac{P}{\rho u^2_{\mathrm{av}}}\end{aligned} \tag{10}$$

It should be noted that these conservation equations for forced convection in the porous region are developed here using the local volume-averaging technique [12].

The associated dimensionless boundary conditions necessary to complete the formulation of the present problem are:

(1) At the entrance ($x^*=0$, $0\leqslant y^*\leqslant 1$)

$$\begin{aligned}&u^*=6y^*(1-y^*),\quad v^*=0,\quad \varphi^*=6\left(\frac{y^{*2}}{2}-\frac{y^{*3}}{3}\right),\\&\xi^*=6(1-2y^*),\quad T^*=0\end{aligned} \tag{11}$$

(2) At the exit ($x^*=L^*$, $0<y^*<1$)

$$\begin{aligned}&\int_0^1 u^*\,\mathrm{d}y^*=1,\quad v^*=0,\quad \frac{\partial\varphi^*}{\partial x^*}=0,\\&\frac{\partial\xi^*}{\partial x^*}=0,\quad \frac{\partial T^*}{\partial y^*}=0\end{aligned} \tag{12}$$

(3) Along the lower plate ($0\leqslant x^*\leqslant L^*$, $y^*=0$)

$$\begin{aligned}&u^*=0,\quad v^*=0,\quad \varphi^*=0,\\&\xi^*=-\frac{\partial^2\varphi^*}{\partial y^{*2}},\quad \frac{\partial T^*}{\partial y^*}=0\end{aligned} \tag{13}$$

(4) Along the upper plate ($0\leqslant x^*\leqslant L^*$, $y^*=1$)

$$\begin{aligned}&u^*=0,\quad v^*=0,\quad \varphi^*=1,\\&\xi^*=-\frac{\partial^2\varphi^*}{\partial y^{*2}},\quad \frac{\partial T^*}{\partial y^*}=0\end{aligned} \tag{14}$$

In addition to these, the three sets of conservation equations are coupled by the following matching conditions at the porous/solid and fluid/porous interfaces [13]:

(5) Along the porous/solid interface (the non-slip condition, and the continuities of temperature and heat flux are accounted)

$$u^* = 0, \quad v^* = 0, \quad T^*_{\mathrm{p}}|_{h(x,y)=0} = T^*_{\mathrm{s}}|_{h(x,y)=0},$$
$$k_{\mathrm{eff}} \left.\frac{\partial T^*_{\mathrm{p}}}{\partial n^*}\right|_{h(x,y)=0} = k_{\mathrm{s}} \left.\frac{\partial T^*_{\mathrm{s}}}{\partial n^*}\right|_{h(x,y)=0} \tag{15}$$

(6) Along the fluid/porous interface (the continuities of the velocity, pressure, stress, temperature, and heat flux are satisfied)

$$u^*_{\mathrm{p}}|_{g(x,y)=0} = u^*_{\mathrm{f}}|_{g(x,y)=0}, \quad v^*_{\mathrm{p}}|_{g(x,y)=0} = v^*_{\mathrm{f}}|_{g(x,y)=0},$$
$$\mu_{\mathrm{eff}} \left.\frac{\partial v^*_{\mathrm{p}}}{\partial n^*}\right|_{g(x,y)=0} = \mu_{\mathrm{f}} \left.\frac{\partial v^*_{\mathrm{f}}}{\partial n^*}\right|_{g(x,y)=0} \tag{16a}$$

$$\mu_{\mathrm{eff}} \left.\left[\frac{\partial u^*_{\mathrm{p}}}{\partial n^*} \frac{\partial v^*_{\mathrm{p}}}{\partial t^*}\right]\right|_{g(x,y)=0} = \mu_{\mathrm{f}} \left.\left[\frac{\partial u^*_{\mathrm{f}}}{\partial n^*} + \frac{\partial v^*_{\mathrm{f}}}{\partial t^*}\right]\right|_{g(x,y)=0} \tag{16b}$$

$$T^*_P|_{g(x,y)=0} = T^*_{\mathrm{f}}|_{g(x,y)=0}, \quad k_{\mathrm{eff}} \left.\frac{\partial T^*_P}{\partial n^*}\right|_{g(x,y)=0} = k_{\mathrm{f}} \left.\frac{\partial T^*_{\mathrm{f}}}{\partial n^*}\right|_{g(x,y)=0} \tag{16c}$$

where $g(x,y) = 0$ and $h(x,y) = 0$ are the curves defining the porous/fluid and porous/solid interfaces, and the derivative with respect to n and t represents the normal and tangential gradients, respectively, to these curves at any point on the interfaces.

To assess the effects of the porous cover on the block heat transfer, the local Nusselt number along the surface of the blocks is evaluated as

$$Nu_x = \frac{hR}{k_{\mathrm{f}}} = -\frac{k_{\mathrm{eff}}}{k_{\mathrm{f}}} \left(\frac{1}{T^*_{\mathrm{s}}}\right) \frac{\mathrm{d}T^*}{\mathrm{d}n^*} \tag{17}$$

where $T^*_{\mathrm{s}} = (T_{\mathrm{s}} - T_{\mathrm{e}})/(Q/k_{\mathrm{f}})$ is the dimensionless block surface temperature and n is the coordinate normal to the block surface. The overall mean Nusselt number for each block is calculated as follow:

$$Nu_{\mathrm{m}} = \frac{\int_{\Pi} Nu_x \, \mathrm{d}\Pi}{\Pi} \tag{18}$$

where Π is the overall exposed area of the block.

3. Numerical method

Employing a non-uniform rectangular grid system, the finite-difference form of the vorticity transport, stream function, and energy equations were derived using control volume integration of these differential equations over discrete cells surrounding the grid points. Fig. 1(b) and (c) shows a typical non-uniform grid system employed for the present calculations. This grid system was designed to capture the steep gradients near the porous/fluid as well as porous/solid interfaces, and to provide sufficient grid density at the solid-block surfaces with minimal element distortion. In the above discretization scheme the upwind and central-differencing formats are introduced for the convective and diffusive terms, respectively. The finite difference equations thus obtained were solved by the extrapolated-Jacobi scheme. This iterative scheme is based on a double-cyclic routine, which translates into a sweep of only half of the grid points at each iteration step [14]. In this work convergence was considered to have been achieved when the absolute value of relative error on each grid point between two successive iterations was found to be less than 10^{-6}.

The interface between the porous medium and fluid space requires special consideration. This is due to the sharp change of thermophysical properties, such as the permeability, porosity, and the thermal conductivity, across the interface. The harmonic mean formulation suggested by Patarkar [15] was used to handle these discontinuous characteristics in the porous/fluid interface. This ensured the continuity of the convective and diffusive fluxes across the interface without an excessively fine grid. In addition, to accommodate the solution of the transport equations in both the fluid and porous regions, the effective viscosity of the fluid-saturated porous medium is set to be equal to the fluid viscosity. It has been found that this approximation provides good agreement with experimental data [16]. In this study, the computational domain was chosen to be larger than the physical domain to eliminate the entrance and exit effects and to satisfy continuity at the exit. A systematic set of numerical experiments was performed to ensure that the use of a fully developed velocity profile for the outflow boundary condition has no detectable effect on the flow solution within the physical domain.

A grid independence study was performed by examining the impact of grid size on overall mean Nusselt number for each solid block. We employed a proper combination of Δx and Δy to assure stability. Three sets of grid systems, 262×110, 392×90, and 730×70, were investigated in this work for a case $Da = 5 \times 10^{-5}$, $\Lambda = 0.35$, $Re = 850$, $L^*_{\mathrm{e}} = 4$, $L^*_{\mathrm{o}} = 14$, $H^*_{\mathrm{p}} = 0.25$, $W^*_{\mathrm{p}} = 0.5$, $S^*_{\mathrm{p}} = 0.5$, $H^*_{\mathrm{s}} = 0.2$, $W^*_{\mathrm{s}} = 0.25$, $S^*_{\mathrm{s}} = 0.75$, $A = 2$, $B = 1$, $k_{\mathrm{s}}/k_{\mathrm{f}} = 10$, and $k_{\mathrm{eff}}/k_{\mathrm{f}} = 1$, $Pr = 0.7$. It is found that there is only less than 1% difference in the overall mean Nusselt number among the solutions for these grid distributions. As this difference is small, all of our computations for the present work were based on the 262×110 grid system.

The mathematical model and the numerical scheme were validated by comparing the present numerical results with three relevant limiting cases available in the literature. The relevant studies for our case correspond to the problems: (1) laminar forced convection in a parallel-plate channel with four strip heat sources in a wall (i.e., $H^*_{\mathrm{p}} = 0$, and $H^*_{\mathrm{s}} = 0$, no porous-covering heat sources) for $W^* = 1$, $S^* = 1$, $L^* = 15$, $Pr = 10$ for $Re = 20$, 100, and 1000; (2) that in a porous channel with

four strip heat sources (i.e., $H_p^* = 1$, $W_p^* \to \infty$ and $H_s^* = 0$), representing the full porous medium case for $\Lambda = 0.1$, $S^* = 1$, $W^* = 1$, $L^* = 15$, $Pr = 10$, and $k_{eff}/k_f = 1$ at $Da = 1 \times 10^{-6}$, and 1×10^{-3} for $Re = 20$, 100, and 1000; and (3) that in a channel with three heated solid blocks (i.e., $Da \to \infty$ and $\varepsilon = 1$, no porous-covering heated block array) for $W_s^* = 0.5$, $H_s^* = 0.25$, $S_s^* = 0.5$, $L_e = 3.0$, $L_o = 9.5$, $Pr = 0.7$, and $k_s/k_f = 10$ at $Re = 100$, 750, and 100. The results for the first and second case, as shown in Fig. 2(a) and (b), agree to better than 1% with data reported by Hardim [9] for overall mean Nusselt numbers. The third validity was to compare with the study of Davalath and Barazitoglu [17] for three heated rectangular blocks in a channel. Comparisons between dimensionless wall temperature distributions along the block exposed faces calculated in [17] and the current analysis show discrepancies less than 1%, as shown in Fig. 2(c).

4. Results and discussion

In this section, the effects of governing physical parameters, such as the Darcy number (Da), inertial parameter (Λ), Reynolds number (Re), and two geometrical parameters ($A = W_p^*/H_p^*$ and $B = S_p^*/W_p^*$) on the flow field, temperature field, local Nusselt number distribution and overall mean Nusselt number were explored. The fixed input parameters for all cases in the simulations were $H_s^* = 0.2$, $W_s^* = 0.25$, $S_s^* = 0.75$, $Le = 4$, $k_s/k_f = 10$, and $Pr = 0.7$ (the cooling fluid in the study is air). Furthermore, the thermal conductivity ratio $R_k = k_{eff}/k_f$ was set equal to 1.0 in order to eliminate the effects of conduction within the porous solid matrix. For illustrating the results of the flow and temperature fields near the heated block array clearly, only this region and its vicinity were presented. However, at all time, the much larger domain was used for numerical calculations and interpretation of the results. In addition, for the sake of brevity, the main features and characteristics of some of the results are discussed and the corresponding figures are not presented.

Fig. 3(a)–(d) displays the effects of a porous-covering block array upon the flow and thermal fields for a baseline case with $Da = 1 \times 10^{-5}$, $\Lambda = 0.35$, $Re = 850$, $Pr = 0.7$, $k_s/k_f = 10$, $k_{eff}/k_f = 1$, $H_p^* = 0.25$, $W_p^* = 0.5$, $S_p^* = 0.5$, $H_s^* = 0.2$, $W_s^* = 0.25$, and $S_s^* = 0.75$. Several interesting features were found from these plots. The streamlines are considerably distorted in the channel due to the presence of the porous-covering block array. The velocity distribution is parabolic at both the entrance and exit of the parallel-plate channel. However, this distribution changes rapidly as the flow is redirected into the bypass region (vena contracta). Although there is no recirculation zone ahead of the first block (but a weak recirculation will appear at larger inertial number or smaller Darcy number), the core flow creates three vortex effects, when it interacts with the porous-covering block array: clockwise recirculations between solid blocks, a relatively strong recirculation behind the last block, and a large anticlockwise eddy zone on the smooth upper plate surface corresponding to the reattached region on the bottom plate. The height of these interblock recirculations is about twice that of the solid blocks, and the extending length of eddy zone also is approximately twice that of the block array. The complicated flowfield within the channel is the results of four interrelated effects: (1) a penetrating effect pertaining to the porous medium; (2) a blowing effect caused by porous medium displacing the fluid from the porous region into the fluid region [18]; (3) a suction effect caused by the adverse pressure behind the porous-covering block, resulting in a downward flow and (4) the effect of boundary-layer separation and reattachment. Downstream of the first cavity, the size, strength, and location of the interblock recirculations appear similar, suggesting possible periodicity. It should be noted that within each interblock cavity, the streamlines between the recirculation center and the upstream wall of that cavity are slightly denser than those between the recirculation center and the downstream wall of the cavity. This shows that the magnitude of upward velocity near the upstream cavity wall is slightly larger than that of the downward velocity near the downstream wall, which may transport more convective energy from the upstream wall than the downstream wall of cavity. In addition, the shape of recirculation zone between two porous-covering blocks is different from that in flow over a cavity. In general, flow over an empty cavity creates a close vortex region (as shown in Fig. 3(e)) and reduces the heat transfer from heated cavity wall, while flow over a cavity formed by two porous-covering blocks produces a recirculating flow, which extends transversely into the core flow and improves fluid mixing. This will enhance the transfer of thermal energy out from the cavity and into the core flow. Hence, the interaction of these recirculations with the core flow plays a significant role in transferring heat from the blocks and in determining temperature distribution in both the fluid and the blocks. Fig. 3(c) shows the isotherms corresponding to the above flow field. The thermal boundary layer thickness increases over the porous-covering block array, and decreases downstream from the block array. Here, the distortion of isotherms arises partly due to the periodical variation in the cross-sectional area of core flow and partly the periodical displacement of fluid from the porous region into the fluid region occurring at the top face of each block. Within each interblock space, spacing between isotherms is closer in the upstream end than in the downstream end. This indicates that a higher temperature

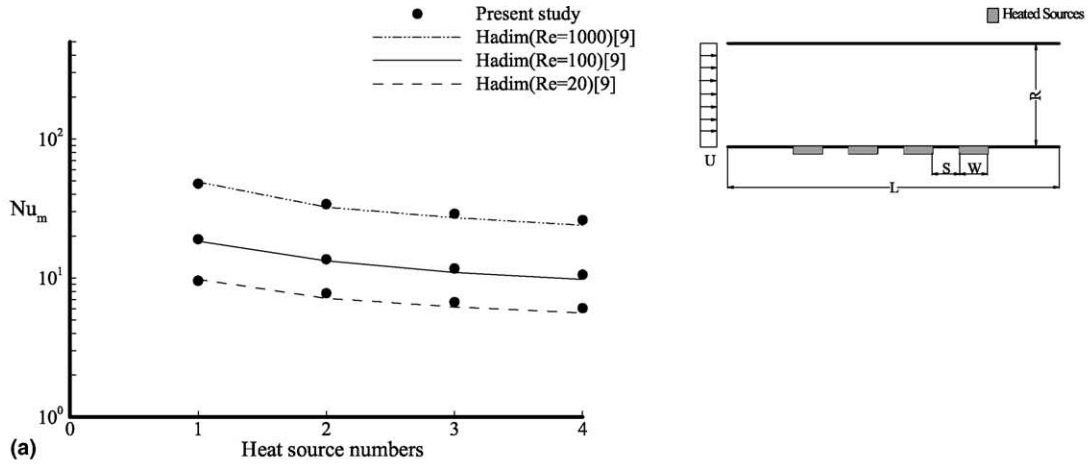

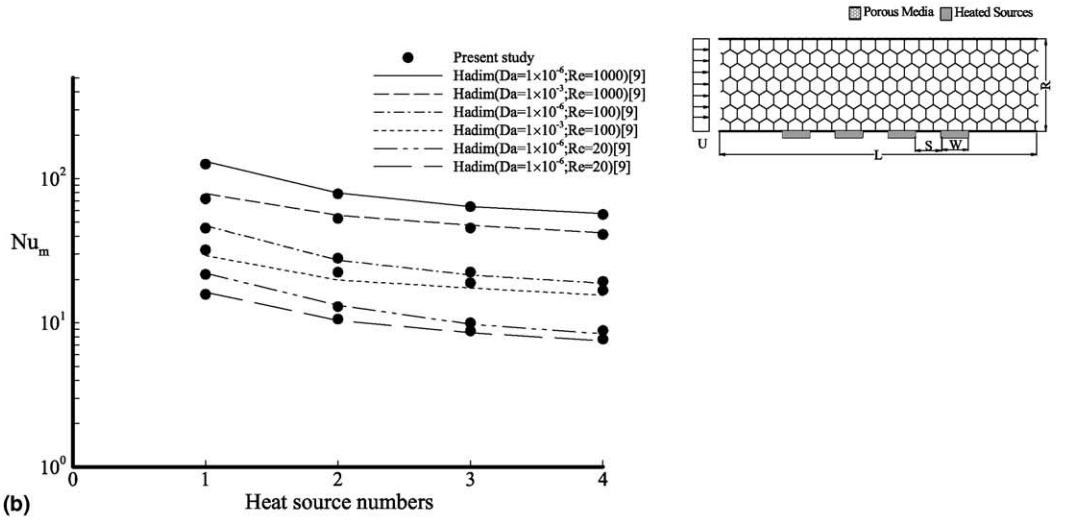

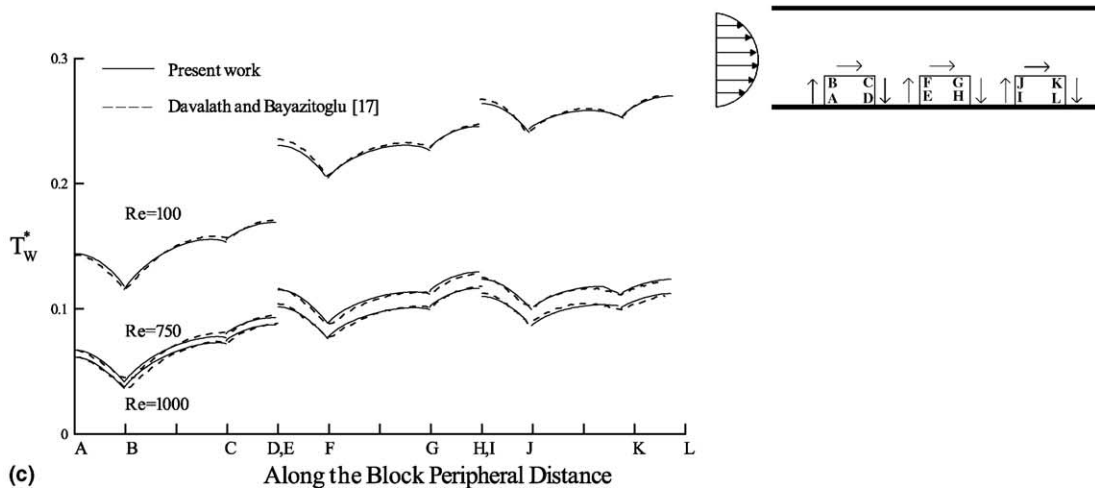

Fig. 2. Comparison of Nu_m on each heat source with that found in [9] for (a) flow in a nonporous channel with various Re, and (b) flow in a full porous channel with various Da and Re. (c) Comparison of T^* along the exposed faces of three heated blocks with the numerical solution given by Davalath and Bayazitoglu [17] for various Re.

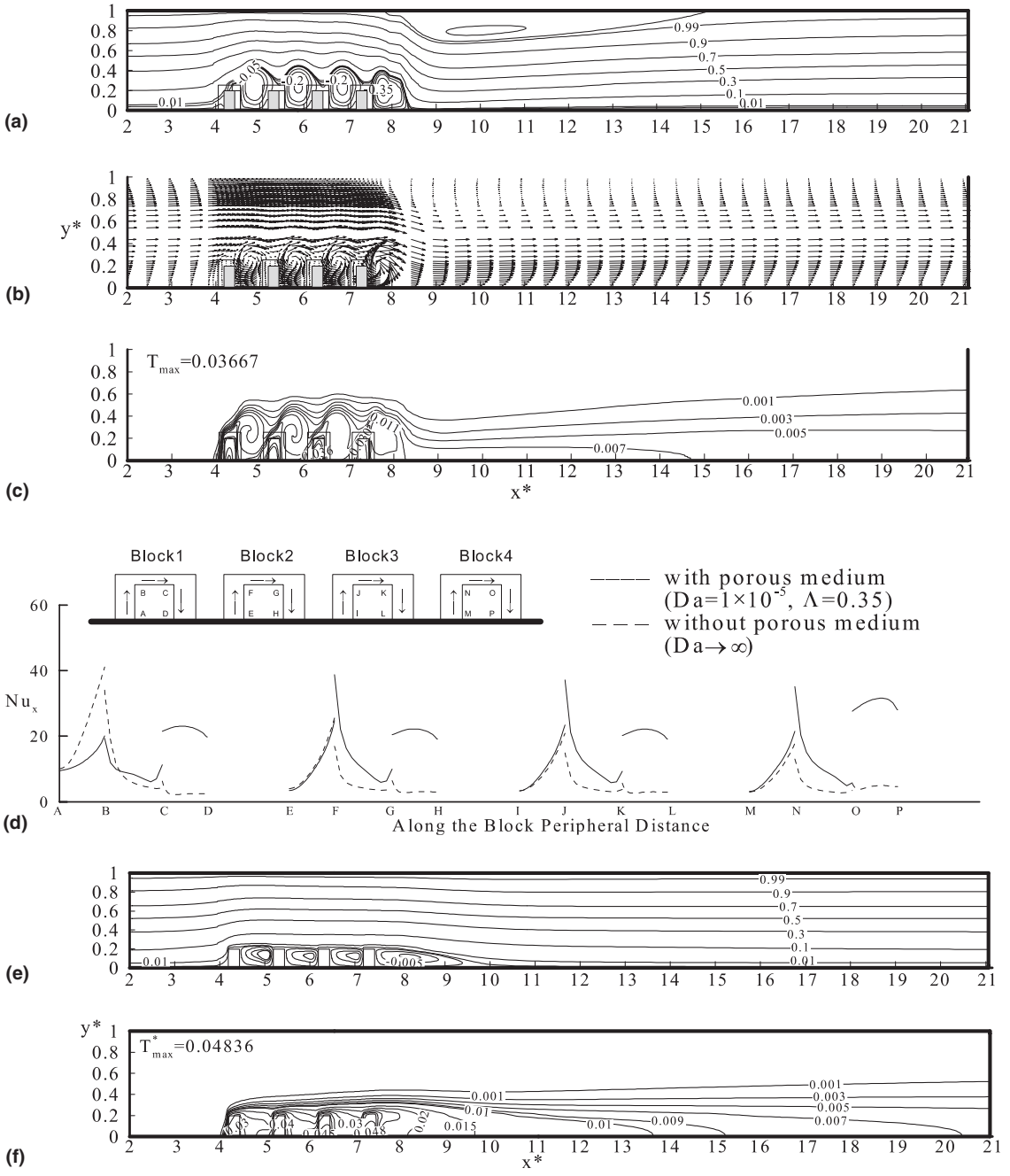

Fig. 3. (a) Streamlines, (b) velocity distribution, (c) isotherms, and (d) local Nusselt number distribution for flow over four porous-covering heated blocks with $Da = 1 \times 10^{-5}$, $\Lambda = 0.35$, $Re = 850$, $Pr = 0.7$, $k_s/k_f = 10$, $k_{eff}/k_f = 1$, $H^*_p = 0.25$, $W^*_p = 0.5$, $S^*_p = 0.5$, $H^*_s = 0.2$, $W^*_s = 0.25$, and $S^*_s = 0.75$. (e) Streamlines, and (f) isotherms for flow over four heated blocks for $Re = 850$, $Pr = 0.7$, $k_s/k_f = 10$, $H^*_s = 0.2$, $W^*_s = 0.25$, and $S^*_s = 0.75$.

gradient in the right face of block than in the left face of proceeding block.

The local Nusselt number distributions around the exposed faces of the four heated blocks for this case is depicted in Fig. 3(d). For a given porous-covering block, along the block left face, Nu_x is small at the lower corner and it grows as the reattachment point is approached due to the recirculation effect. The maximum Nu_x occurs

at the upper corner. For the top face, the Nu_x is largest at the left corner and then decreases rapidly to a local minimum value. Near the (block top) right corner Nu_x increases slightly. This can be explained by noting that since this surface is parallel to the flow direction, as the fluid turns around the corner, a thermal boundary layer starts to develop at the left corner. Under the blowing effect caused by porous matrix attached to that surface, the thickness of thermal boundary layer grows up quickly. Downstream the top face, the boundary-layer separation occurs, resulting in an increase in the convective energy transport again due to the fluid mixing. Along the block right face, the better heat transfer can be found on the face. Here the heat dissipated is carried away via the recirculating flow discussed previously.

For the left, top, and right faces in the heated block array, Nu_x decreases slightly for downstream blocks except block one. The reason is that as the fluid passed over the blocks, the temperature of the fluid increases. Consequently, the temperature difference between the fluid and the block decreases as the fluid moves downstream; as a result, the local Nusselt number decreases progressively for downstream blocks. The last block in the array has largest Nu_x values along its right face than the other ones. This is because the recirculating flow is in the clock direction, the frontal side of a block is cooled before the rear side of the previous block and there is no heat-generating block behind this face. The first block has largest Nu_x values along the left face than the downstream blocks, except the small region near the left upper corner of the block, due to the impact of the core flow as it is redirected into the bypass region (vena contracta) and lower temperature gradient near the left upper corner of block. While block one has smallest Nu_x values along the top face than the other blocks, except near the top right corner where the momentum boundary-layer separation occurs. This is because of the higher temperature gradient near the top left corner for second and successive blocks than for first block under the action of inter-block recirculation. Comparison of local Nusselt number distributions for the block array with and without porous cover shows that the extension-transverse recirculating flow caused by porous medium can augment significantly the heat transfer rate from the block faces, especially in both right and top faces of second and subsequent blocks, to the core flow by convection, as illustrated in Fig. 3(d). As for block 1, the Nu_x values along the left face (AB) are lower for the case with porous cover. The reason is that the porous matrix constitutes a resistance to the flow, which diminishes both the strength of lower corner possible vortex and the impaction of core flow on this face and in turn reduces the convective energy transport. Along the top face (BC), for the porous case Nu_x is lower on the forward part of face wall and become larger on rear part of face. This is because there is a less steep velocity gradient in the fluid as it turns around the leading-edge corner of the top face and the separation flow at some downstream distance. In addition, Fig. 3(c) and (f) predicts that the maximum temperature in the porous-covering block array is reduced by up to 24% in comparison with the pure block array.

4.1. Effect of Darcy number

The Darcy number, $Da = K/R^2$, is directly related to the permeability of the porous medium. To investigate the effect of Darcy number on flow and temperature fields, computations were carried out at $Da = 5\times10^{-4}$, 9×10^{-5}, 3×10^{-5}, 8×10^{-6}, 1×10^{-6}, and 0, respectively, for $H_p^* = 0.25$, $W_p^* = 0.5$, $S_p^* = 0.5$, $\Lambda = 0.35$, and $Re = 850$. The flow fields displayed in Fig. 4(a) reveal that as Darcy number decreases from 5×10^{-4} to 3×10^{-5}, the distortion of streamlines and the size of recirculations behind the blocks become more pronounced. Meanwhile a relative larger vortex is formed along the top channel wall downstream the heated block array. While as Da is decreased further to 0, an opposite tendency is found. When Da approaches to zero (the solid block with porous medium could be regarded as a simple solid block), there are no streamlines penetrating the porous covers, the core flow passes over the solid block array and a closed vertex is formed within each interblock cavity. In other words, there exists a critical Darcy number corresponding to the largest recirculation height, and below or above this value the recirculation height drops off. This is the result of four competing effects of penetrating, blowing, suction, boundary layer separation and reattachment, as discussed in the previous section. Fig. 4(b) displays how Nu_x distributions around the block surfaces changes with Darcy number. In the range of $5\times10^{-4} \geqslant Da \geqslant 3\times10^{-5}$ for the right and left faces of second and subsequent blocks, Nu_x increases with decreasing Da (until an optimal DA/heat transfer rate is reached) due to the stronger interaction between the core flow and the interblock recircultion flow, which can convect more thermal energy away from the block. Along the top faces of the same blocks, as Da decreases, the increasing tendency of local Nusselt number distribution from a local maximum value at the left corner to a local minimum value near the right corner is more steeper, whereas an opposite result occurs for the block one. This phenomenon is due to the fact that a smaller value of Da translates into larger blowing effects, which in turn increases the increment of thermal-boundary-layer thickness for downstream block one. The maximum value of Nu_x occurring at the leading edge of top face increases with decreasing Da due to the larger temperature gradient caused by the larger recirculation flow ahead of the block. Near the top right corner,

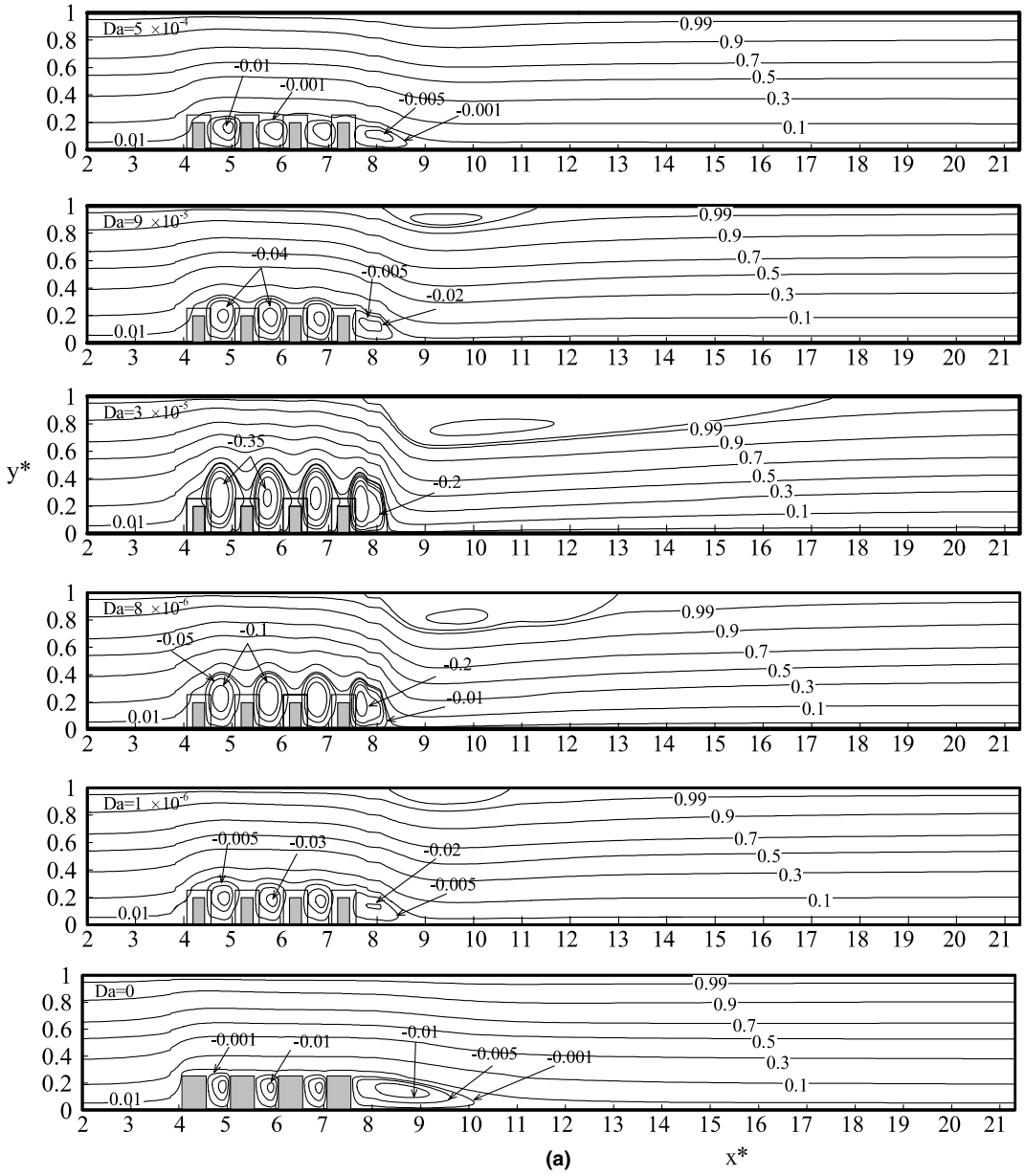

Fig. 4. Effects of the Darcy number on (a) streamlines and (b) local Nusselt number distributions and (c) overall mean Nusselt number.

Nu_x decreases to a local minimum value and then increase slightly. This increased level becomes more significant for smaller Da due to the stronger separation flow downstream the top face. For the first block, Nu_x decreases along the left and top faces as Da decreases because of the smaller impact of core flow on the left face and the smaller temperature gradient at the leading-edge corner of the top face as the fluid turns upwards and accelerates into the bypass region. Whereas, along its right face, Nu_x increases with decreasing Da due to the larger recirculation behind it. As Da further decreases to 0, the opposite variation occurs for Nu_x distributions versus Da. This is due to the weaken interaction between the core flow and the recirculation, which in turn diminish the convective energy transport away from the blocks.

The effects of Da on Nu_m over each heated block are shown in Fig. 4(c). As expected, there exists an optimum Da for which the heat transfer rate is maximum. Any increase or decrease in Da will result in the decreases of Nu_m.

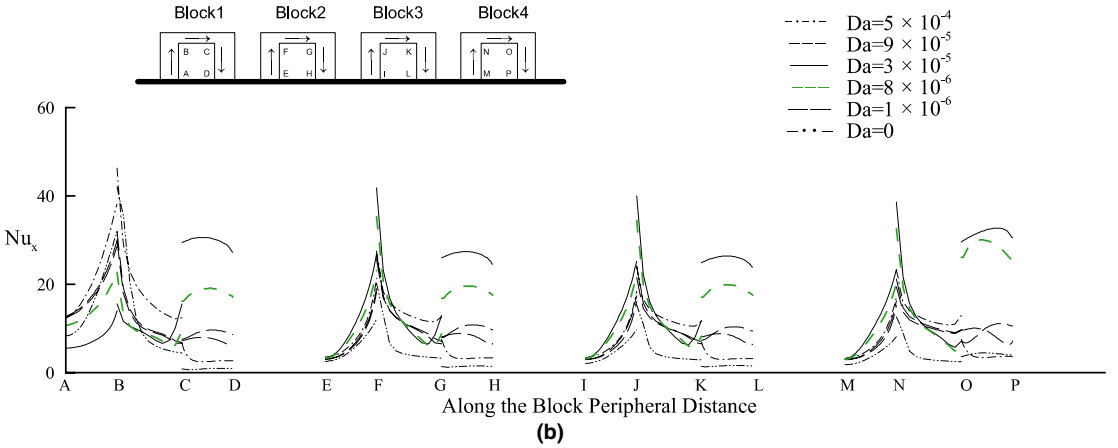

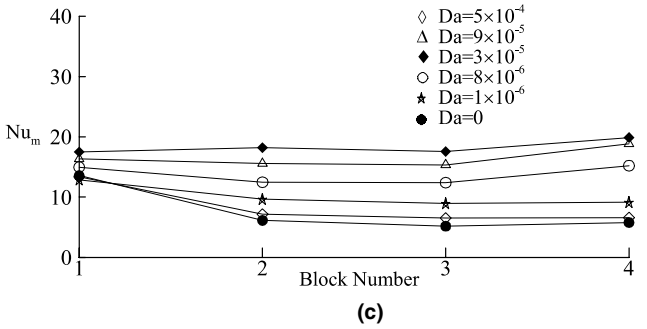

Fig. 4 (*continued*)

4.2. Inertial effects

The inertial parameter $\Lambda = FR\varepsilon/\sqrt{K}$ is concerned with microstructure of the porous solid matrix, which causes an increase in the inertial effects at higher velocity [12]. The effect of an increase or decrease in the inertial parameter Λ is shown in Fig. 6 for $H_p^* = 0.25$, $W_p^* = 0.5$, $S_p^* = 0.5$, $Da = 5 \times 10^{-5}$, $Re = 850$, $k_s/k_f = 10$, and $k_{eff}/k_f = 1$, with $\Lambda = 0.35$, 11 and 21. Comparison of the streamlines in Fig. 5(a) shows that the distortion of streamlines and the size of recirculation zones become pronounced as the inertial parameter increases. This is because the larger bulk frictional resistance that the flow experiences for larger inertial parameters. Therefore, larger value of Λ would lead to a larger blowing effect through porous substrate, especially in block top face, which displaces the fluid deeper into the core flow, and creates larger interblock and downstream recirculation zones. Comparison of the corresponding isotherms shows that the larger the value of Λ, the more noticeable the distortion of the isotherms due to the size increase of the recirculation zones within the flowfield. As in the case of Darcy number variations, both heat transfer enhancement in the top and right faces of second and subsequent blocks and heat transfer retardation in the left and top faces of the first block are observed. As can be seen in Fig. 5(b), for larger inertial parameters Nu_x along the right faces of each block increase, slightly increases along the left and top faces of second and subsequent blocks, and decreases along the left and top faces of the first block due to the larger recirculation flows before and behind the block. This is similar to the effect of Darcy number on the local Nusselt number distribution. It should be noted that Nu_x decreases with increasing inertial parameter along the right face of last block. This is because the temperature difference between the fluid and the last block decreases as the inertial parameter increases, which decreases the transfer of thermal energy out from this face into the core flow. As expected, the block overall mean Nusselt number increases with an increase in the inertial parameter, except for last block (as shown in Fig. 5(c)).

4.3. Effect of Reynolds number

The effect of variations in the Reynolds number is depicted in Fig. 6 for $H_p^* = 0.25$, $W_p^* = 0.5$, $S_p^* = 0.5$, $Da = 5 \times 10^{-5}$, $\Lambda = 0.35$, $k_s/k_f = 10$, and $k_{eff}/k_f = 1$ with

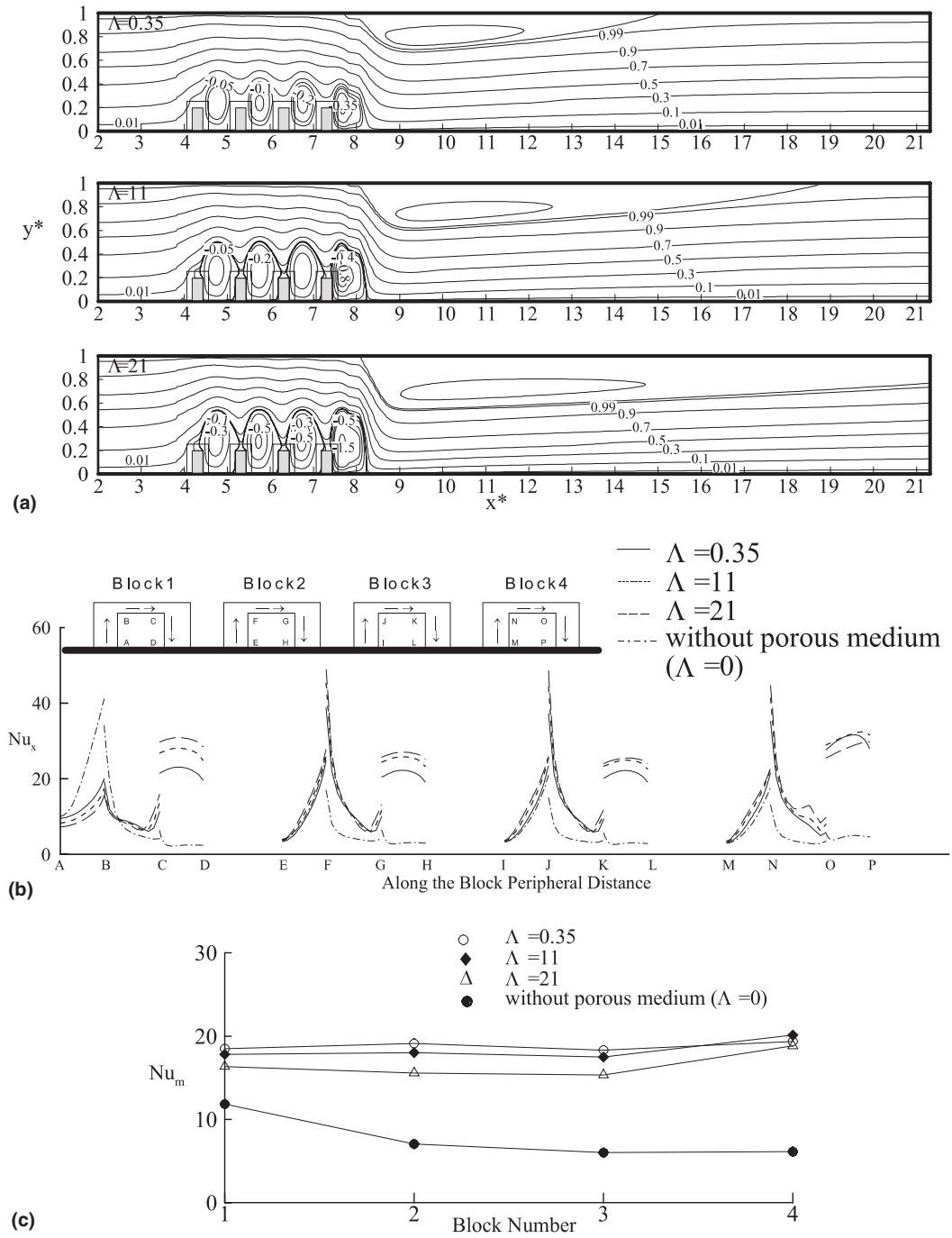

Fig. 5. Effects of the inertial number on (a) streamlines, (b) local Nusselt number distributions (c) overall mean Nusselt number.

Re = 600, 850, and 1500, respectively. The flowfields displayed in the Fig. 6(a) shows that the extent of the distortion in the core and the area of interblock recirculation zone decrease as the Reynolds number increases. The reason for this trend is that increasing *Re* increases the fluid's forward momentum, resulting in a larger penetration into the porous matrix. This, in turn, reduces the action of the blowing effect caused by porous medium on the block top face and restrains the expansion of recirculation flows in the transverse direction. In addition, as *Re*

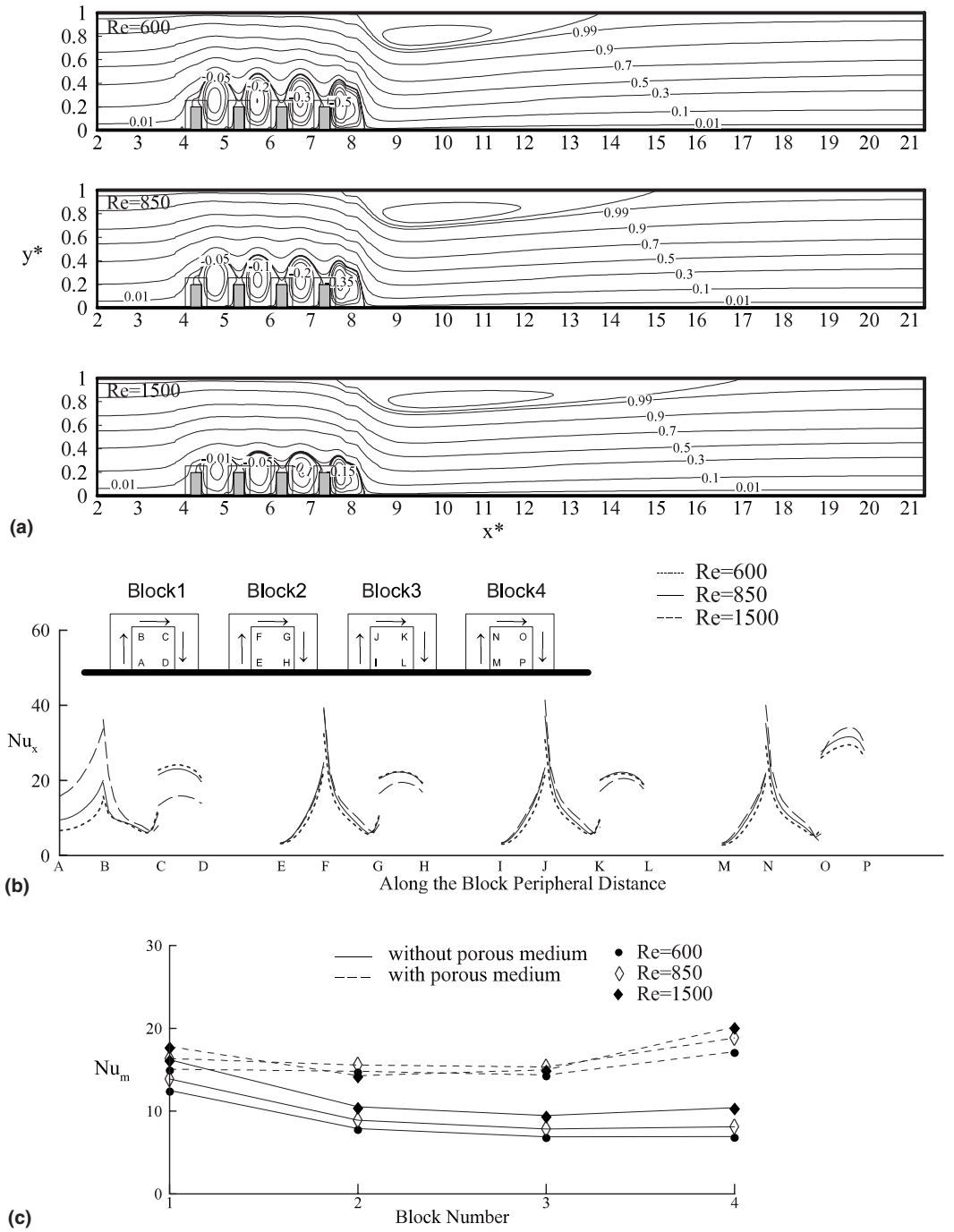

Fig. 6. Effects of the Reynolds number on (a) streamlines, (b) local Nusselt number distributions and (c) overall mean Nusselt number.

increases the area of downstream vortex zone attaching on the upper plate extends axially and the size of the weak vortex zone ahead of the first block decreases. As expected, the distortion of isotherms in the channel region corresponding the flow field becomes smoother with an increase in *Re*. Fig. 6(b) shows the effects of *Re* on the Nu_x distributions around the four block faces. For each block top faces, the heat transfer rate from the top faces slightly increase as the Reynolds number increases. This is due to the higher velocities near the top face for larger Reynolds number, which is able to convect more thermal energy away from the face. Along the left and right faces,

for larger Re the first block has much larger Nu_x values along its left face because of the larger impact of core flow as it turns upwards and accelerates into the bypass region. The last block has also larger Nu_x value along its right face because of the larger temperature difference between the fluid and the block as the fluid moves downstream. The remaining vertical faces within the block array, the Nu_x decreases along the block right face and slightly increases along the block left face as Re increases from 600 to 1500. The thermal transport from these faces is dominated by the interblock recircuations. The larger the value of Re, the smaller the recirculation zone, which decreases convective heat transfer from these block faces. Meanwhile, the core flow, through increasing axial momentum, pushes the centers of recirculation to downstream wall of cavity. Fig. 6(c) gives the results for overall block mean Nusselt numbers. It can be seen that as Re increases Nu_m increases. As Re increase up to 1500, Nu_m decreases for second and third blocks, which is the direct result of the described flow field. As expected, the maximum temperature in the block array decreases with increased Re.

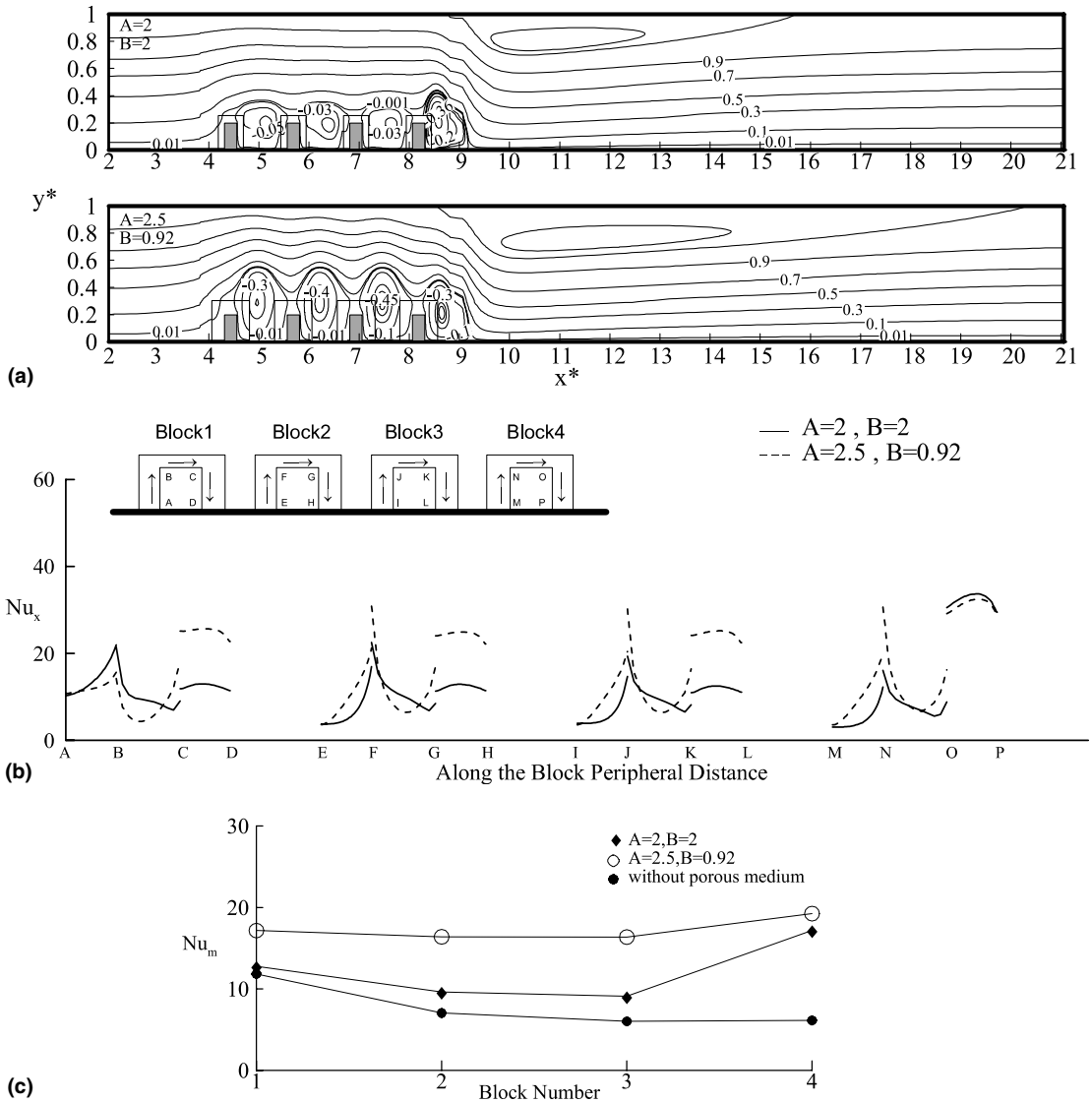

Fig. 7. Effects of the geometric parameters A on (a) streamlines, (b) local Nusselt number distributions, and (c) overall mean Nusselt number.

4.4. Effects of the geometric parameters A and B

The geometric parameters A and B are related to the aspect ratio of the porous cover and the interspacing between porous covers. The effect of aspect ratio on the flow and temperature fields were studied for $Da = 5 \times 10^{-5}$, $\Lambda = 0.35$, $Re = 850$, $k_s/k_f = 10$, $k_{eff}/k_f = 1$, $Pr = 0.7$, $H_s^* = 0.2$, $W_s^* = 0.25$, and $S_s^* = 1.25$. The

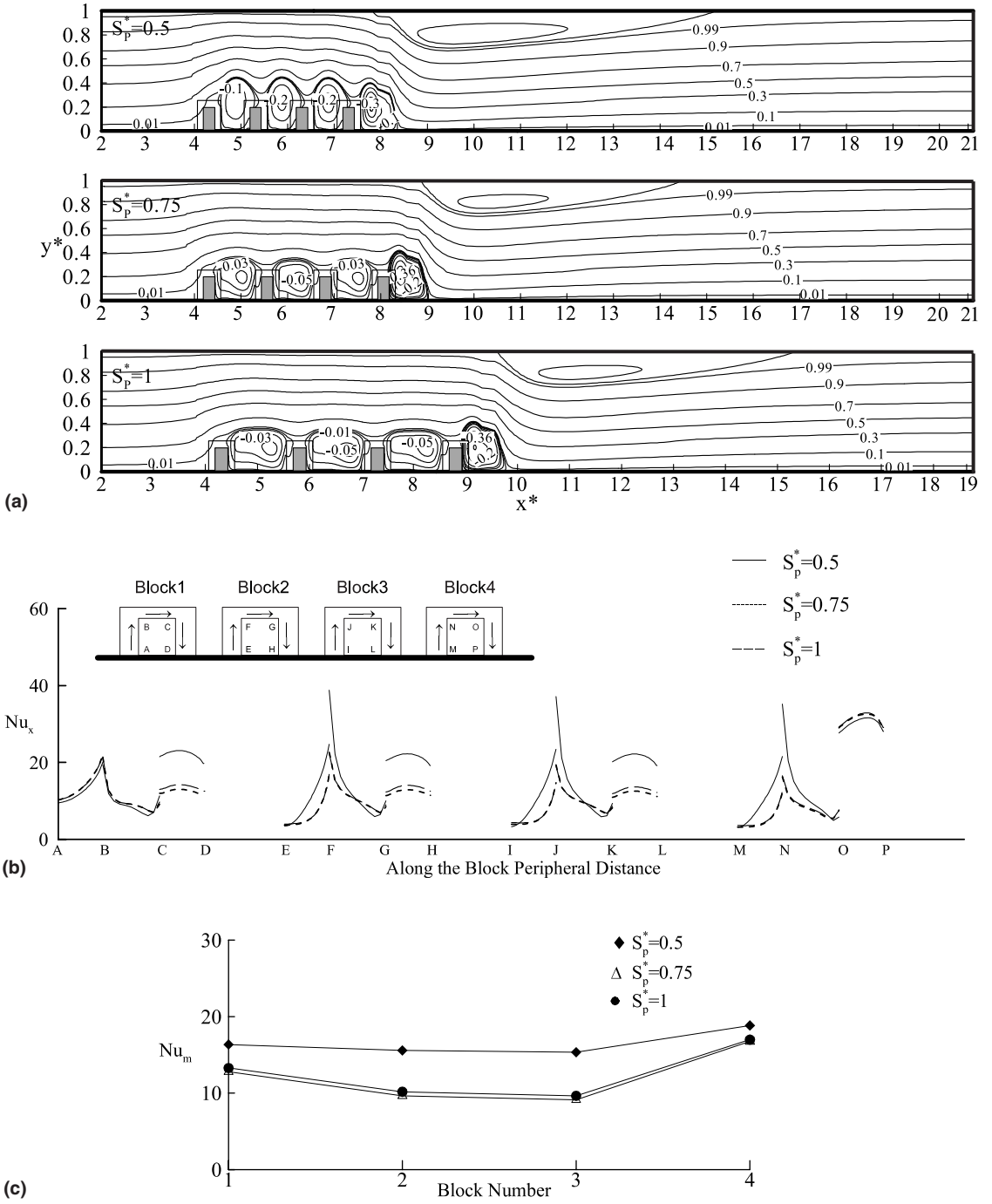

Fig. 8. Effects of the geometric parameters B on (a) streamlines, (b) local Nusselt number distributions, and (c) overall mean Nusselt number.

streamlines for $A = 2$ (i.e., $H_p^* = 0.25$ and $W_p^* = 0.5$), $B = 2$ and $A = 2.5$ (i.e., $H_p^* = 0.3125$ and $W_p^* = 0.7812$), $B = 0.92$ are represented on Fig. 7. As can be seen that the distortions for streamlines become evident. In addition, the size and strength of recirculation zones increase. This is the direct result of the uniform-ratio increase in the porous-covering thickness around the block surfaces, which in turn offers a higher degree of obstruction to the flow and subsequent grows the blowing action.

The effects of increasing the porous-covering block spacing in the arrays from $B = 1$ to $B = 2$ (i.e., $s_p^* = 0.5$, 0.75, and 1.0) are shown in Fig. 8 for $A = 2$ (i.e., $H_p^* = 0.25$, $W_p^* = 0.5$), $Da = 5 \times 10^{-5}$, $\Lambda = 0.35$, $Re = 850$, $Pr = 0.7$, $k_s/k_f = 10$, $k_{eff}/k_f = 1$ $H_s^* = 0.2$, and $W_s^* = 0.25$. The wider block spacing produces the flatter-and-wider interblock recirculation, whose center moves to downstream wall of interblock cavity. This is because the larger block spacing allows more fluid into the interblock cavity, which, in turn, causes acceleration in the core flow and lessens the blowing action maded by porous medium. Fig. 7(b) and Fig. 8(b) show the variation of Nu_x with geometric parameters A and B, respectively. As expected, the larger interblock recirculation produces higher heat transfer rate from the block left (EF, IJ, MN) and right (CD, GH, KL) faces to the core flow by convection, but reduces at the block top faces (BC, FG, JK). It is noticed that the relative large recirculating cell in front of the first block reduces the local Nusselt number along its left face. As shown in Fig. 7(c) and Fig. 8(c), the block overall mean Nusselt numbers increase with increased porous-covering size but decrease with increased porous-covering block spacing.

4.5. Effects of the porous cover on the pressure drop

When using a porous material for heat transfer enhancement, an important factor to consider is the pen-

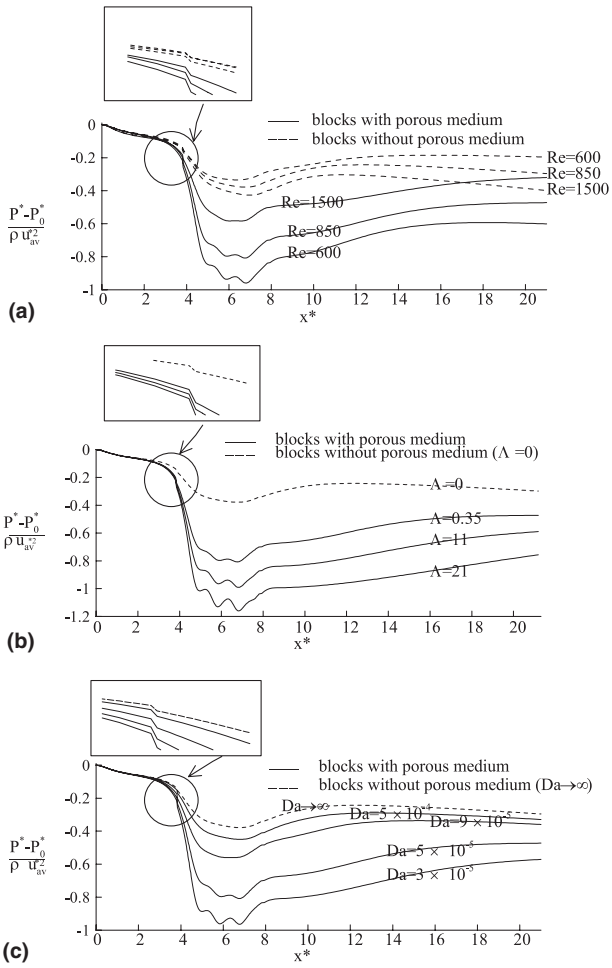

Fig. 9. Effects of (a) Reynolds number, (b) inertial parameter, and (c) Darcy number on the pressure drop along the upper plate for $Pr = 0.7$, $k_s/k_f = 10$, $k_{eff}/k_f = 1$, $H_p^* = 0.25$, $W_p^* = 0.5$, $S_p^* = 0.5$, $H_s^* = 0.2$, $W_s^* = 0.25$, $S_s^* = 0.75$.

alty arising from increased pressure drop. In the stream function-vorticity formulation, the pressure field is eliminated in obtaining the solution. However, the pressure field can be recovered from the converged stream function and vorticity fields. This is done by integrating the pressure gradient along the upper channel wall. The pressure gradient is derived from the momentum equation using the no-slip boundary conditions on the solid wall. The total pressure drop along the upper channel wall is then obtained from

$$\int_0^{L^*} \left.\frac{\partial P^*}{\partial x^*}\right|_{y^*=1} \mathrm{d}x^* = \frac{P^*_{L^*} - P^*_0}{\rho u^{*2}_{\mathrm{av}}} = -\int_0^{L^*} \frac{1}{Re} \left.\frac{\partial \xi^*}{\partial y^*}\right|_{y^*=1} \mathrm{d}x^*, \tag{19}$$

where pressure P^* is non-dimensionalized with respect to $\rho u^{*2}_{\mathrm{av}}$.

Fig. 9(a) depicts that the effect of Reynolds number on the pressure distribution along the upper plate wall for a channel containing four blocks with and without the porous cover for $Da = 5 \times 10^{-5}$, $\Lambda = 0.35$, $Pr = 0.7$, $H^*_{\mathrm{s}} = 0.2$, $W^*_{\mathrm{s}} = 0.25$, $S^*_{\mathrm{s}} = 0.75$, $H^*_{\mathrm{p}} = 0.25$, $W^*_{\mathrm{p}} = 0.5$, $S^*_{\mathrm{p}} = 0.5$, $k_{\mathrm{s}}/k_{\mathrm{f}} = 10$, and $k_{\mathrm{eff}}/k_{\mathrm{f}} = 1$. It can be seen that both block-array cases cause an increase in the total pressure drop. This is mainly due to the fact that as the flow approaches the smaller passage formed by the block and the upper surface of the channel, the fluid starts to accelerate, resulting in an increase in the pressure drop. Pressure recovery behind each block is not complete due to pressure loss in the recirculation zones. In addition, the eddy on the upper plate delays the pressure recovery behind the last porous-covering block. For the channel with porous-covering block array, the dimensionless pressure drop decreases with an increase in the Reynolds number. This is because the pressure drop rate decreases across the smaller recirculation zones. Whereas, the trend is reversed at the channel with pure solid block array due to the increases in size and strength of up- and downstream recirculation zones and interblock vortices with increasing Re.

Pressure drop increases with the inertial number for $Re = 850$, $Da = 5 \times 10^{-5}$, $Pr = 0.7$, $H^*_{\mathrm{s}} = 0.2$, $W^*_{\mathrm{s}} = 0.25$, $S^*_{\mathrm{s}} = 0.75$, $H^*_{\mathrm{p}} = 0.25$, $W^*_{\mathrm{p}} = 0.5$, $S^*_{\mathrm{p}} = 0.5$, $k_{\mathrm{s}}/k_{\mathrm{f}} = 10$, and $k_{\mathrm{eff}}/k_{\mathrm{f}} = 1$, as portrayed in Fig. 9(b). The reason is that the larger the recirculation zones, the larger the pressure drops for flow across the block array. The influence of Darcy number on the magnitude of the pressure drop along the upper plate wall is displayed in Fig. 9(c) for $\Lambda = 0.35$, $Re = 850$, $H^*_{\mathrm{s}} = 0.2$, $W^*_{\mathrm{s}} = 0.25$, $S^*_{\mathrm{s}} = 0.75$, $H^*_{\mathrm{p}} = 0.25$, $W^*_{\mathrm{p}} = 0.5$, $S^*_{\mathrm{p}} = 0.5$, $k_{\mathrm{s}}/k_{\mathrm{f}} = 10$, and $k_{\mathrm{eff}}/k_{\mathrm{f}} = 1$. It can be seen that the computed pressure distribution becomes more distorted across the porous-covering block array for lower Darcy number and pressure drop increases with decreasing Da. This is due to stronger vorticity gradients which exist for lower Darcy numbers.

5. Conclusion

A comprehensive investigation of forced convection cooling enhancement of multiple heated blocks discrete mounted in a parallel-plate channel using porous covers has been presented in this work. Parametric numerical simulations have been performed to capture the fundamental and practical results. The rectangular porous-covering block array changes the incoming parabolic velocity field considerably, resulting in the formation of vortices zones between the blocks. The transverse height of these vortices has significant effects on the heat transfer characteristics around the exposed faces of the blocks. The dependence of flow and temperature fields on parametric changes in the governing parameters, Darcy number, inertia parameter, Reynolds number, and two geometric parameters, is documented. The results of this investigation show that the shape and matrix of the porous cover shall markedly enhance the heat transfer rate on both right and top block faces of second and subsequent. Comparison of the overall mean Nusselt number with and without porous cover for the four-block array clearly shows that significant cooling augmentation of the blocks can be achieved through the cover of finite-sized porous substance.

Acknowledgments

The first author gratefully acknowledges the support of the National Science council of the Republic of China through contact No. NSC 90-2212-E-027-012.

References

[1] A.D. Kraus, A. Barcohen, Thermal Analysis and Control of Electronic Equipment, McGraw-Hill, 1983.
[2] S.J. Kim, S.W. Lee, Air Cooling Technology for Electronic Equipment, CRC Press, New York, 1996.
[3] J.C.Y. Koh, R. Colony, Analysis of cooling effectiveness for porous material in a coolant passage, ASME J. Heat Transfer 96 (1974) 324–330.
[4] M. Kaviany, Laminar flow through a porous channel bounded by isothermal parallel plate, Int. J. Heat Mass Transfer 28 (1985) 851–858.
[5] P.C. Huang, K. Vafai, Analysis of forced convection enhancement in a channel using porous blocks, AIAA J. Thermophys. Heat Transfer 18 (1994) 563–573.
[6] J.M. Zhang, W.H. Sutton, F.C. Lai, Enhancement of heat transfer using porous convection-to-radiation converter for laminar flow in a circular duct, Int. J. Heat Mass Transfer 40 (1997) 39–48.

[7] S.M. Kuo, C.L. Tien, Heat transfer augmentation in a foam-material filled duct with discrete heat sources, in: Proceedings of the Thermal Phenomena in Electronics Components Conference, Los Angeles, CA, May 11–13, 1988.
[8] T. Rizk, C. Kleinstreuer, Forced convective cooling of a linear array of blocks in open and porous matrix channels, Heat. Transfer Eng. 12 (1991) 4–47.
[9] A. Hadim, Forced convection in a porous channel with localized heat sources, ASME J. Heat Transfer 8 (1994) 465–472.
[10] Y. Ould-Amer, S. Chikh, K. Bouhadef, G. Lauriat, Forced convection cooling enhancement by use of porous materials, Int. J. Heat Fluid Flow 19 (1998) 251–258.
[11] M.L. Hunt, C.L. Tien, Effects of thermal dispersion on forced convection in fibrous media, Int. J. Heat Mass Transfer 31 (1988) 301–310.
[12] K. Vafai, C.L. Tien, Boundary and inertial effects on flow and heat transfer in porous media, Int. J. Heat Mass Transfer 24 (1981) 195–203.
[13] K. Vafai, S.J. Kim, Analysis of surface enhancement by a porous substrate, ASME J. Heat Transfer 112 (1990) 700–705.
[14] J. Adams, A.J. Ortega, A multicolor SOR method for parallel computation, in: Proceedings of the International Conference on Parallel Procession, 1982, pp. 53–56.
[15] S.W. Patanker, Numerical Heat Transfer and Fluid Flow, McGraw-Hill, New York, 1980.
[16] T.S. Lundgren, Slow flow through stationary random beds and suspensions of spheres, J. Fluid Mech. 51 (1972) 273–299.
[17] J. Davalath, Y. Bayazitoglu, Forced convection cooling across rectangular blocks, ASME J. Heat Transfer 109 (1987) 321–328.
[18] P.C. Huang, K. Vafai, Flow and heat transfer control over an external surface using a porous block array arrangement, Int. J. Heat Mass Transfer 36 (1993) 4019–4032.